

## RESEARCH ARTICLE

10.1002/2013JD020558

## Key Points:

- The TTL is identified using the ozone and water vapor relationship
- The tracer TTL is consistent with the CPT and LMS as upper and lower boundaries
- The transition layer in the Asian monsoon region is compared to the TTL

## Correspondence to:

L. L. Pan,  
liwen@ucar.edu

## Citation:

Pan, L. L., L. C. Paulik, S. B. Honomichl, L. A. Munchak, J. Bian, H. B. Selkirk, and H. Vömel (2014), Identification of the tropical tropopause transition layer using the ozone-water vapor relationship, *J. Geophys. Res. Atmos.*, 119, 3586–3599, doi:10.1002/2013JD020558.

Received 14 JUL 2013

Accepted 6 NOV 2013

Accepted article online 11 NOV 2013

Published online 28 MAR 2014

## Identification of the tropical tropopause transition layer using the ozone-water vapor relationship

Laura L. Pan<sup>1</sup>, Laura C. Paulik<sup>1,2</sup>, Shawn B. Honomichl<sup>1</sup>, Leigh A. Munchak<sup>1,2</sup>, Jianchun Bian<sup>3</sup>, Henry B. Selkirk<sup>4</sup>, and Holger Vömel<sup>5</sup>
<sup>1</sup>National Center for Atmospheric Research, Boulder, Colorado, USA, <sup>2</sup>Now at Science Systems and Applications, Inc., Lanham, Maryland, USA, <sup>3</sup>Key Laboratory of Middle Atmosphere and Global Environment Observation, Institute of Atmospheric Physics, Chinese Academy of Sciences, Beijing, China, <sup>4</sup>Goddard Earth Sciences and Technology Center, University of Maryland Baltimore County, Baltimore, Maryland, USA, <sup>5</sup>GRUAN Lead Center, Meteorologisches Observatorium, Lindenberg, Germany

**Abstract** We present a method of identifying the tropical tropopause transition layer (TTL) using chemical tracer-tracer relationships. Coincident ozone (O<sub>3</sub>) and water vapor (H<sub>2</sub>O) measurements over Alajuela, Costa Rica (~10°N), in July and August 2007 are used to demonstrate the concept. In the tracer-tracer space, the O<sub>3</sub> and H<sub>2</sub>O relationship helps to separate the transition layer air mass from the background troposphere and stratosphere. This tracer relationship-based transition layer is found to span an approximately 40 K potential temperature range between 340 and 380 K and is largely confined between the level of minimum stability (LMS) and the cold point tropopause (CPT). This chemical composition-based transition layer is, therefore, consistent with a definition of the TTL based on the thermal structure, for which the LMS and CPT are the lower and upper boundaries of TTL, respectively. We also examine the transition layer over the region of Asian summer monsoon (ASM) anticyclone using the measurements over Kunming, China (~25°N), and compare its behavior with the TTL structure in the deep tropics. The comparison shows that the transition layer over the ASM is similar to the TTL, although the data suggest the ASM transition layer lies at higher potential temperature levels and is potentially prone to the influence of extratropical processes.

## 1. Introduction

Although the troposphere and the stratosphere are separated by the tropopause, the thermodynamic transition from the troposphere to the stratosphere in the tropics occurs in a layer of several kilometers [Highwood and Hoskins, 1998]. Most notably, a change in vertical stability occurs at ~12 km, near the level of the maximum meridional velocity of the Hadley cell [Palmén and Newton, 1969]. To note the significance of this change, Palmén and Newton [1969] named this level the secondary tropical tropopause (STT). The layer between STT and the thermal tropopause (here the differences between the cold point tropopause (CPT) and the lapse rate tropopause (LRT) are neglected) near 16–17 km is later defined as the tropical tropopause layer (TTL) [Haynes and Shepherd, 2001; Sherwood and Dessler, 2001]. Alternatively, the TTL is also defined as the tropical transition layer [Holton and Gettelman, 2001]. Note that the concept of the tropical transition layer has a longer history, extending almost two decades before the TTL was formally defined [Atticks and Robinson, 1983; Highwood and Hoskins, 1998]. For the remainder of the paper, we will use the acronym “TTL” interchangeably to describe this region.

A significant body of work in the last decade has focused on the study of TTL, motivated largely by the need to better understand stratospheric water vapor trends. From the chemical transport perspective, it was recognized that the properties of the TTL, instead of the CPT, control the water vapor transport into the stratosphere [Holton and Gettelman, 2001; Sherwood and Dessler, 2001; Folkins, 2002; Fueglistaler et al., 2009]. Over the last decade, studies of the thermodynamical, chemical, and microphysical structure of the TTL have expanded to include, for example, the role of convective transport in the upper tropospheric and lower stratospheric chemical composition, how it couples to the Brewer-Dobson circulation in the lower stratosphere, and competing transport processes, such as the Asian summer monsoon (ASM) circulation.

This work is motivated, foremost, by the need for a better conceptual understanding of the TTL. In particular, although the existence of two TTL definitions, the tropical tropopause layer [Sherwood and Dessler, 2001] and the tropical transition layer [Holton and Gettelman, 2001], is acknowledged [Fueglistaler et al., 2009], the conceptual differences between the two are generally obscure. The motivation of this work is to examine the physical implications of the definitions using chemical tracer observations.

The distinction between definitions of the TTL is most readily defined in terms of the upper and lower boundaries. Although the TTL boundaries are stated in broad terms in many published works, the following two are the best described definitions and reflect the two subtly different conceptual models. A mass flux-based definition has been described and reiterated by Folkins [2002], Fu et al. [2007], and Fueglistaler et al. [2009], hereafter the “mass-flux definition.” A temperature structure-based definition has been proposed and described in Gettelman and de F. Forster [2002], hereafter the “thermal definition.”

The mass-flux definition defines a “tropical tropopause layer” (i.e. a layer that serves as a boundary), across which the air mass on average enters the stratosphere. The lower and upper boundaries of this TTL were first estimated to be 356 K (~15.0 km) and 375 K (~16.6 km) in recognition of the fact that in this region, the mass fluxes for the Hadley (tropospheric) and Brewer-Dobson (stratospheric) circulations are of comparable magnitude [Folkins, 2002]. These levels were later refined based on radiative mass flux calculations [Fu et al., 2007]. The lower boundary was redefined to be the tropically averaged level of zero net radiative heating for full sky (150 hPa or 14 km) [Fueglistaler et al., 2009] and the upper boundary was redefined to be the level at which the local mass flux becomes comparable to that of the Brewer-Dobson circulation (70 hPa or 18.7 km) [Fu et al., 2007] (Note that the zero net radiative heating for full sky is significantly different from that of the clear sky conditions, ~14 km versus 15.5 km, see Fueglistaler et al. [2009] for citations). These boundaries are based on averaged conditions that utilize both local (e.g., temperature and wind at the upper boundary) and nonlocal (e.g., radiative heating from tropical mean cloud distribution) information.

The thermal definition defines a “tropical transition layer” (i.e., a layer that is a transition zone), in which the background thermodynamic structure transitions between the convectively dominated troposphere and the radiatively controlled stable stratosphere. In this definition, the boundaries are identified by the temperature profiles and derived lapse rates: The cold point tropopause and the level of minimum stability are defined as the upper and lower boundaries, respectively. This definition follows the long history of tropical observations [Palmén and Newton, 1969; Atticks and Robinson, 1983; Highwood and Hoskins, 1998; Haynes and Shepherd, 2001] that lead to the formal definition of the TTL. The boundaries in this case are locally defined and can be derived from instantaneous measurements.

The goal of this work is to examine the relationship between the vertical structure of the chemical tracers and the thermal and dynamical boundaries of the TTL. Using the chemical tracers, we aim to identify a chemically “measurable” TTL, i.e., a physical layer within which the air mass composition is distinct from the troposphere below and the stratosphere above. The boundaries of this layer should therefore be marked by the change of the air mass’ chemical composition. We examine the layer so defined in relation to the thermally and dynamically defined TTL boundaries. This analysis directly shows whether a defined boundary appears to be physical, i.e., marks the discontinuity in chemical composition and is therefore relevant to chemical transport.

The approach we use is the method of tracer-tracer correlation, which has been successful in identifying the transition layer in the extratropics [Fischer et al., 2000; Hoor et al., 2002; Pan et al., 2004, 2007a, 2007b; Hegglin et al., 2009]. In this work we explore the application of the method in the tropics. This is an empirical method derived from the observed generally compact relationship between a stratospheric tracer and a tropospheric tracer in the tracer-tracer space across the upper troposphere and lower stratosphere (UTLS). This relationship is approximately “L” shaped, with a compact tracer-tracer relationship for the stratospheric and tropospheric air masses, which are often referred to as “the stratospheric branch” and “the tropospheric branch,” respectively. The transition between the two branches defines the shape of the corner of the L. An air mass’ position in the tracer-tracer space provides its identity, i.e., whether it belongs to the stratosphere, to the troposphere, or should be considered transitional. When combining this analysis with the geometric space and dynamical information, it is an effective way to identify where the transition happened and what dynamical structure is associated with an air mass boundary.

We use ozone ( $O_3$ ) and water vapor ( $H_2O$ ) from balloon soundings for tracer correlation analyses because this type of measurement has sufficient vertical sampling range in both the stratosphere and troposphere.  $O_3$  is used as a stratospheric tracer and  $H_2O$  as a tropospheric tracer. The vertical profiles of both tracers are found to be a useful indicator of convection in the tropics [Kley *et al.*, 1996, 2007; Folkins *et al.*, 2002]. While most previous studies have used the average behavior of these trace gas profiles, we use the correlative relationship of the pair and examine their structure relative to the colocated dynamical boundaries.

It has been recognized in recent years that the ASM anticyclone is a significant transport pathway for water vapor and pollutants to enter the stratosphere, bypassing the tropical tropopause [Dethof *et al.*, 1999; Randel *et al.*, 2010]. Recently, paired  $O_3/H_2O$  soundings of the ASM region have become available [Bian *et al.*, 2012]. These data allow us to pursue an additional goal of this work, which is to compare and contrast the characteristics of the transition layer in the deep tropics with the ASM region, which is outside the tropics if using the geographic latitude criterion. In particular, we are interested to find if dynamically consistent definitions of the TTL apply in these two dynamically distinct regions.

## 2. Data From Two Selected Campaign Locations

The  $O_3$  and  $H_2O$  data used in this analysis are from Cryogenic Frostpoint Hygrometer (CFH) and electrochemical concentration cell (ECC) ozonesondes from ground-based balloon-borne soundings. The payload also includes various models of Vaisala radiosondes. Thus, these measurements provide profiles of water vapor, ozone, pressure, temperature, and wind from the surface up to  $\sim 25$  km altitude. The CFH  $H_2O$  uncertainty is estimated to be  $\sim 10\%$ . Detailed descriptions are given in Vömel *et al.* [2007]. The ECC ozonesonde is described by Komhyr [1969]. The ozone uncertainty is typically within 5–10% but is estimated to be larger ( $\sim 10$ –15%) in the tropical tropopause region [Smit *et al.*, 2007]. The original sounding data have  $\sim 10$  m vertical sampling intervals. For our analyses, the profiles are processed by a binned average at 250 m intervals. This filtering removes high-frequency noise in the data and creates a regular altitude grid.

This analysis uses  $O_3$  and  $H_2O$  data from two field campaigns. The first data set is from the Tropical Composition, Cloud and Climate Coupling Experiment (TC<sup>4</sup>), which was a multi-aircraft research campaign conducted during July and August 2007 [Toon *et al.*, 2010]. During the experiment, 16 pairs of CFH/ECC water vapor and ozone payloads were launched from Alajuela, Costa Rica ( $10^\circ N$ ,  $84.2^\circ W$ ). Of these, 14 provided coincident soundings of  $H_2O$  and  $O_3$  up to the cold point and contributed to this analysis. The details of the launch conditions and associated experimental specifics are given in Selkirk *et al.* [2010].

The second data set is from the Sounding Water Vapor, Ozone, and Particle (SWOP), which was a multiyear ground-based sounding campaign in the ASM region. Eleven pairs of  $H_2O/O_3$  soundings from Kunming, China ( $25.0^\circ N$ ,  $102.7^\circ E$ ) from the first phase of this project in August 2009 are used in this analysis. Specifics of the Kunming experiment and the launch conditions can be found in Bian *et al.* [2012].

The two campaign locations are significantly different geographically which translates to very different climatological backgrounds. Alajuela is a near-equatorial tropical location and located in the Central Valley of Costa Rica at an elevation of 890 m. In this work, we consider the location as representative of the “deep tropics.” Kunming, China, on the other hand, is a subtropical location on Yungui Plateau at an elevation of 1890 m. The UTLS structure over Kunming is tropical during boreal summer, as indicated by the high tropopause (shown later in Figure 2), which is also consistent with the seasonal location of the ITCZ [e.g., Lawrence and Lelieveld, 2010, Figure 5]. In this work, we refer to the location as “ASM” and contrast the UTLS behavior of this region with that in the “deep tropics.” In relation to the ASM UTLS dynamical structure, Kunming is at the southeast edge of the anticyclone [Bian *et al.*, 2012]. While the anticyclone is dynamic and displays intraseasonal variability, data analysis reveals that the soundings are mostly measured inside of the anticyclone. These factors should be kept in mind when comparing the two groups of soundings.

## 3. Temperature, Ozone, and Water Vapor Profiles

We begin the analysis with the temperature profiles and background thermodynamical structure. Theory and modeling studies suggest that the temperature structure in the tropical lower atmosphere represents radiative-convective equilibrium [Held, 1982; Thuburn and Craig, 2000]. As part of the radiative-convective balance, the top of the convective influence is often several kilometers below the cold point. A transition

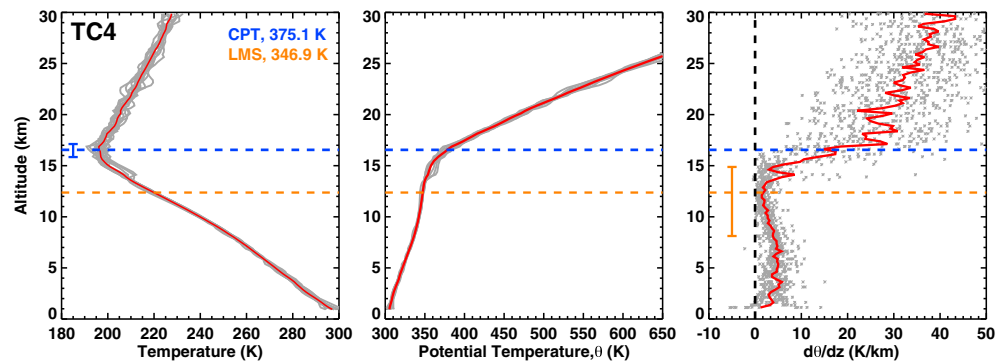
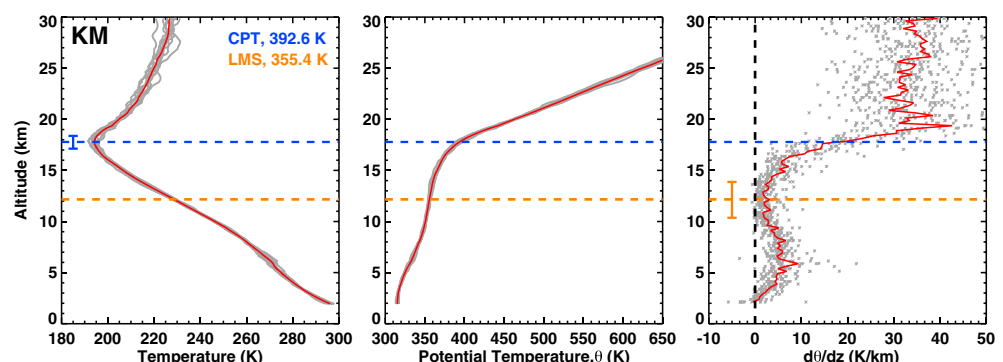


**Figure 1.** TC<sup>4</sup> campaign (2007, Alajuela) temperature ( $T$ ), potential temperature ( $\theta$ ) and static stability (as represented by  $d\theta/dz$ ) profiles. In each profile, two critical levels can be identified: the cold point tropopause (CPT) is identified by the temperature minimum and the level of the minimum stability (LMS) is identified by the minimum of  $d\theta/dz$ . The mean CPT and LMS levels are shown as the blue and orange dash lines, respectively. The red lines indicate the mean profiles. A total of 14 profiles is included.

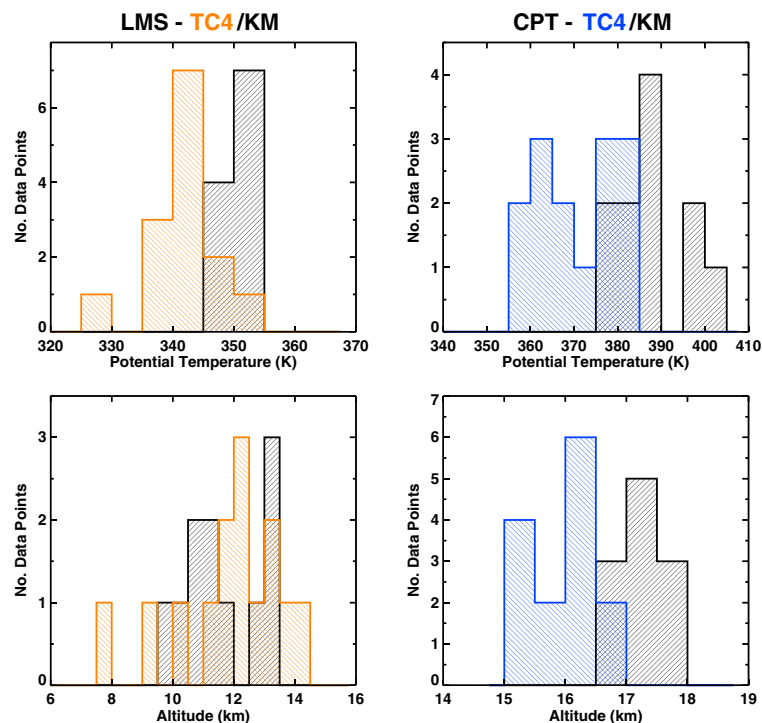
layer extends from the top of the convection to the cold point, influenced by both stratospheric and tropospheric processes [Thuburn and Craig, 2002]. The cold point tropopause marks a sharp increase in stability, above which the potential temperature profile is close to radiative equilibrium. The level of minimum stability marks the departure from the convective equilibrium and has been considered as the secondary tropical tropopause [Palmén and Newton, 1969; Atticks and Robinson, 1983; Gettelman and de F. Forster, 2002]. Note that this level in general is below the level of neutral buoyancy (LNB) [Paulik and Birner, 2012], which is associated with the level of maximum detrainment and the upper extent of convective cloud tops [Folkins, 2002; Takahashi and Luo, 2012].

Figure 1 displays the temperature ( $T$ ), potential temperature ( $\theta$ ), and the derived potential temperature gradient profiles ( $d\theta/dz$ , instead of the lapse rate profile,  $-d\theta/dz$ ) for the 14 TC<sup>4</sup> profiles. Using these thermal profiles, the two levels that separate the above mentioned dynamical regions are readily identified: the CPT by the minimum in the temperature profile and the level of minimum stability (LMS) by the minimum of  $d\theta/dz$  profile. The averages and the ranges of variability (as represented by the minimum and maximum) for the two levels are also shown in Figure 1. The  $T$  profiles are fairly compact, resulting in an average CPT altitude of 16.6 km and a CPT potential temperature of 375.1 K. (Note a much larger set of measurements over the same time period is discussed in Pfister *et al.* [2010]. The CPT altitude reported there is  $16.8 \pm 0.7$  km and the average CPT  $\theta$  was  $379.7 \pm 13$  K.) The LMS shows greater variability, but averages to an altitude of 12.4 km (346.9 K). This is consistent with a known feature for the deep tropics and has been shown to be consistent with the sea surface equivalent potential temperature distributions [Folkins *et al.*, 1999; Folkins, 2002].

As a contrast for the ASM region, Figure 2 shows  $T$ ,  $\theta$ , and  $d\theta/dz$  profiles from the Kunming soundings. The structure of the Kunming profiles shares common features with that of the Alajuela profiles. In particular, the Kunming profiles have a well-defined CPT in the altitude range of the tropical tropopause, i.e., higher than



**Figure 2.** Same as Figure 1 but for the 2009 Kunming data. A total of 11 profiles is included.



**Figure 3.** Distributions of the LMS and the CPT in potential temperature and altitude. In each panel,  $TC^4$  distribution is shown in color, and Kunming distribution is shown in black.

15 km defined in *Seidel and Randel* [2007], indicating that the ASM region, although geographically outside the tropics, is “tropical-like” in summer. The static stability profiles show pronounced differences between the two regions in the stratosphere. The Alajuela profiles have a gradual increase in stability above the CPT, while the Kunming profiles have significantly higher stability right above the CPT and relatively constant stability for several kilometers of altitude into the lower stratosphere. This latter behavior is known to be a characteristic of the subtropics [*Birner*, 2006; *Grise et al.*, 2010].

The most striking difference between the two regions, however, is the much higher average potential temperature and altitude of the CPT in the Kunming profiles. While the average CPT temperatures are similar, the Kunming CPT potential temperature and altitude averages are approximately 17 K and 1 km higher than  $TC^4$ /Alajuela. This is also a known feature [*Dethof et al.*, 1999] that makes the vertical transport in ASM an effective pathway to bypass the tropical tropopause and acting as a competing pathway. While the LMS at Alajuela is typical of a tropical location, the level of main convective outflow in the ASM region is not

well known and is a subject of ongoing research. In this small data set, the Kunming LMS is approximately 355 K, ~10 K higher than the  $TC^4$ /Alajuela measurements.

Because both of the data sets contain a relatively small number of profiles, it is helpful to look at the distributions. Figure 3 shows the altitude and potential temperature distributions of the CPT and LMS for the two data sets. It appears that the distribution of LMS is more compact in potential temperature space and CPT levels are more compact in the altitude space. This is consistent

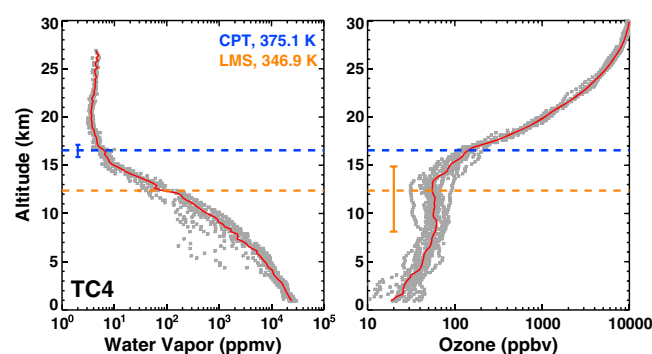


**Figure 4.** Water vapor and ozone mixing ratio profiles from Alajuela during  $TC^4$  on August 2007. The red line represents the mean profile.

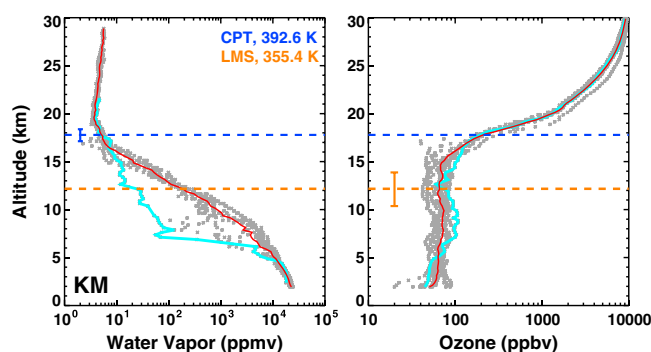


**Figure 5.** Water vapor and ozone profiles from Kunming on August 2009. The red line represents the mean profile. An anomalous profile sampled on 7 August is shown in cyan. For details see section 5.

levels. While these profiles were previously published [Selkirk *et al.*, 2010], they are included here to provide a conceptual link between physical space and the tracer-tracer relationships shown later. Similarly, Kunming profiles, shown in Figure 5, were also previously published [Bian *et al.*, 2012], which includes the comparisons of the two sets of profiles (TC<sup>4</sup>/Alajuela and SWOP/Kunming) with a focus on the H<sub>2</sub>O profiles. The mean H<sub>2</sub>O profiles from the two data sets are similar. The stratospheric H<sub>2</sub>O distributions (375–500 K potential temperature range) from the two data sets largely overlap with each other. The stratospheric O<sub>3</sub> profiles are also very similar in the two data sets. The most notable difference between the two data sets is the tropospheric ozone distribution and the “shape” of the upper troposphere ozone profiles. The Kunming data set shows a higher tropospheric O<sub>3</sub> mixing ratio, which is discussed later in section 4. The shapes of the two tropospheric mean ozone profiles are also different. The TC<sup>4</sup> profile is approximately “s” shaped (or “seahorse” shaped), with a clear decrease near and above the LMS. This feature is not clearly present in the Kunming mean profile. This type of upper tropospheric ozone minima is known to be the result of convection, especially over an oceanic boundary layer [Folkins *et al.*, 2002]. The ozone minimum is an indication of the main convective outflow level. Although both campaigns measured convective influence, the different boundary layer ozone levels, which are apparent in Figures 4 and 5, are largely responsible for the different mean profile shapes.

Note that there is an anomalous profile (indicated in cyan in Figure 5) in Kunming soundings that is particularly evident in the water vapor profile (Figure 5, left). The dynamical condition that contributed to the anomalous middle tropospheric behavior is discussed later.

#### 4. Method of Determining Transition Layer Using Tracers

As documented in previous studies, in the tracer-tracer space, the UTLS O<sub>3</sub> and H<sub>2</sub>O form an L-shaped relationship [e.g., Pan *et al.*, 2007a, 2007b]. This relationship provides an effective diagnostic for identifying the transition across the tropopause based on air masses’ chemical composition. This method has been used to identify tropopause transition layers in the extratropics. In this section we demonstrate the application of this method for identifying the tropical tropopause transition layer using the O<sub>3</sub> and H<sub>2</sub>O data from the two data sets.

The general concept is that relative to the troposphere, the lower stratosphere H<sub>2</sub>O has small variability due to the lack of sources (here we consider the H<sub>2</sub>O production from methane oxidation to be negligible in the LS). Similarly, tropospheric O<sub>3</sub> has small variability relative to the stratosphere. The small variability of stratospheric tracers in the troposphere and tropospheric tracers in the stratosphere is a key factor leading to the compact L-shaped relationship of the two tracers in the UTLS. The compact relationship serves as the basis for analyzing the troposphere to stratosphere transitional behavior near the corner of the L, where the tracer relationship departs from the stratospheric and tropospheric relationship.

The empirical separation between the background air mass, i.e., the air masses that form the stratospheric or tropospheric branches of the L, and the air mass influenced by mixing between the two layers, in general, requires the specification of maximum values of the stratospheric tracer (O<sub>3</sub>) in the troposphere and the

with the behavior of temperature and potential temperature profiles in these two regions—LMS is the region of near constant potential temperature so the minimum gradient in this region can potentially vary over a large altitude range. The CPT has a very well defined altitude from the temperature profiles, but it is a region where potential temperature has a large gradient.

Figure 4 shows TC<sup>4</sup> H<sub>2</sub>O and O<sub>3</sub> profiles from Alajuela, including 14 individual soundings and the mean profile. Also displayed are the mean CPT and LMS

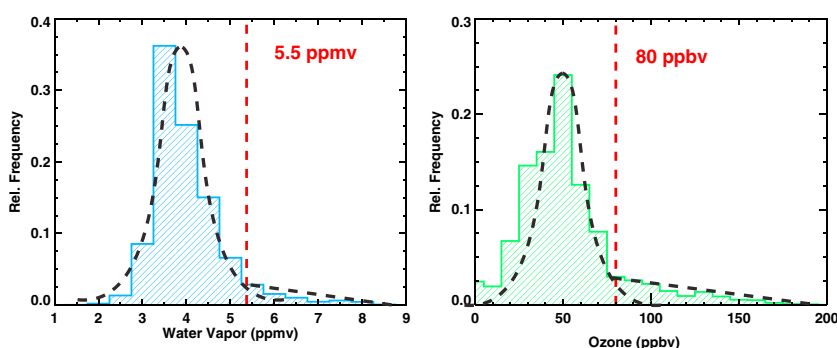


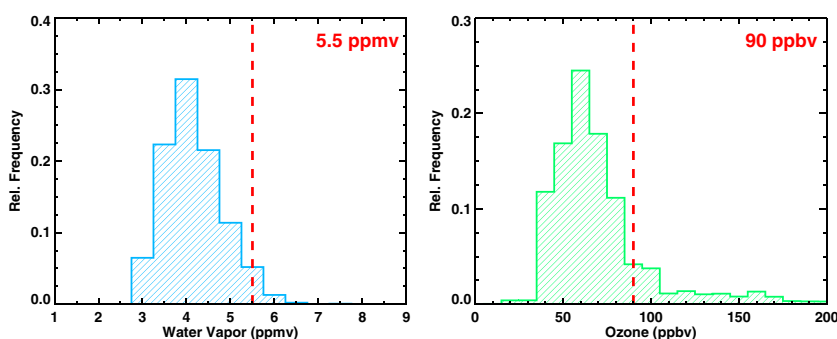
**Figure 6.** Distributions of stratospheric water vapor mixing ratios and tropospheric ozone mixing ratios from the measurements. Black dash curves indicate the conceptual model of the background approximated by a Gaussian function, and in-mixing air mass from the other side of the tropopause shown as the tail. The intersection point is chosen as the upper limit of stratospheric (tropospheric) background air mass using water vapor (ozone), indicated by the red dash line. In this case, the cutoff is chosen to be 5.5 ppmv of  $\text{H}_2\text{O}$  and 80 ppbv of  $\text{O}_3$ .

tropospheric tracer ( $\text{H}_2\text{O}$ ) in the stratosphere. Figure 6 demonstrates a conceptual model of how the choices of maximum values are made using distributions of stratospheric  $\text{H}_2\text{O}$  and tropospheric  $\text{O}_3$  from the  $\text{TC}^4$  data. The stratospheric (tropospheric) data points are selected as above (below) the CPT.

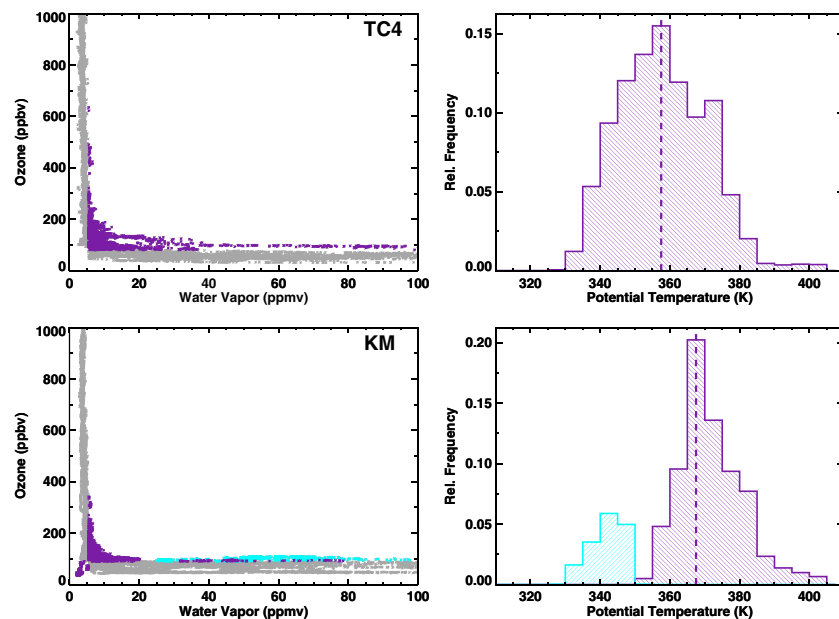
As shown in the figure, the distributions of both tropospheric  $\text{O}_3$  and stratospheric  $\text{H}_2\text{O}$  may be approximated by a Gaussian distribution with a “tail.” Conceptually, the Gaussian distribution represents the background and the tail on the high-value side of the distribution indicates the influence of the mixing from the other side of the tropopause. We choose the critical value from the point where the tail intersects the Gaussian curve. Due to small sample size, the Gaussian curves (and the outlier lines) shown in Figure 6 were not derived mathematically but were fit by eye to illustrate the concept. The intersecting points of the two populations are approximately at 5.5 ppmv of  $\text{H}_2\text{O}$  and 80 ppbv of  $\text{O}_3$ . We designate the two upper limits to be  $\text{H}_2\text{O}_s$  and  $\text{O}_{3t}$ . Subsequent analyses show that the final result is relatively insensitive to small variations of the cutoff values (see section 6).

Figure 7 shows the distribution and selection of critical values for the Kunming campaign data, using the same method although the Gaussian curve and a tail are not shown on the figure. The result shows that  $\text{H}_2\text{O}$  provides similar cutoff value ( $\text{H}_2\text{O}_s = 5.5$  ppmv) for the stratospheric background. The  $\text{O}_3$  distribution, however, shows a higher cutoff value ( $\text{O}_{3t} = 90$  ppbv) for Kunming, possibly the result of a more polluted background.

Based on the cutoff values, the background stratospheric/tropospheric parcels and transitional air mass are separated as shown in Figure 8. Specifically, the tropospheric background is selected by  $\text{O}_3 < \text{O}_{3t}$  and  $\text{H}_2\text{O} > \text{H}_2\text{O}_s$ . The stratospheric background is selected to be  $\text{O}_3 > \text{O}_{3t}$  and  $\text{H}_2\text{O} < \text{H}_2\text{O}_s$ . In the tracer space, the transitional air mass appears near the corner of the L with concentrations in general above the cutoff values



**Figure 7.** Stratospheric water vapor and tropospheric ozone distributions for the Kunming data set. The red dashed line indicates the choice of cutoff values.



**Figure 8.** (left column)  $\text{O}_3$ - $\text{H}_2\text{O}$  relationship in the vicinity of the tropopause and (right column) the tracer-based transition layer in potential temperature space for  $\text{TC}^4$  and Kunming. In the left column, background and transitional air masses are color coded in gray and purple, respectively. The right column show the potential temperature distribution of the air mass identified as part of the transition layer (the purple/cyan points from the left column). The tropospheric background is selected by  $\text{O}_3 < \text{O}_{3t}$  and  $\text{H}_2\text{O} > \text{H}_2\text{O}_s$ . The stratospheric background is selected by  $\text{O}_3 > \text{O}_{3t}$  and  $\text{H}_2\text{O} < \text{H}_2\text{O}_s$ .  $\text{O}_{3t}$  and  $\text{H}_2\text{O}_s$  are the tropospheric and stratospheric cutoff values shown in Figures 6 and 7. The points in cyan are identified transitional air mass from the anomalous profile (Kunming 7 August sounding) and will be discussed in section 5.

for both tracers. A small group of measurements from a single sounding contributed to air masses that appear in  $\text{O}_3 < \text{O}_{3t}$  and  $\text{H}_2\text{O} < \text{H}_2\text{O}_s$  part of the tracer-tracer space. A trajectory study attributes this anomalous profile to the influence of convective lifting over the western Pacific and it has been discussed in *Bian et al.* [2012].

In the potential temperature space, the transitional air mass forms a layer of approximately 40 K. The layers from the two data sets show appreciable differences. The  $\text{TC}^4$  transition layer has its maximum frequency around 360 K and spans 340–380 K. The frequency of the Kunming transition layer peaks near 370 K and spans approximately 360–390 K. There is a smaller group of parcels distributed below 350 K (cyan section in Figure 8). This segment consists of measurements from a single sounding obtained on 7 August (cyan in the tracer space and profiles in Figure 5). As we discuss later, there is a clear indication that these measurements sampled a midlatitude stratospheric filament.

Note that the use of cutoff values for stratospheric and troposphere tracers is a simplified scheme compared to the method presented in *Pan et al.* [2004], where the relationships of tracers that belong to selected stratospheric/tropospheric air masses are further modeled by a linear or quadratic function. In that case, the air parcels belonging to the compact relationship, often called stratospheric or tropospheric “branch” in the L-shaped relationship, are filtered by using standard deviation from the fit to the function. We were able to employ a simplified cutoff in these analyses because the relationship is very compact and linear within the range of interest for these data. Also note that these cutoff values are based on the local measurements. Although these values are representative, we do not consider them to be universally applicable. The specific criteria for identifying stratospheric and tropospheric background should be derived using specific data sets that are relevant to the given investigation.

## 5. Transition Layer Relative to the Thermodynamical Boundaries

To relate the tracer-defined transition layer to the thermal structure, we aggregate the identified transitional air masses in vertical coordinates relative to the critical levels in the thermal structure. Figure 9 shows the

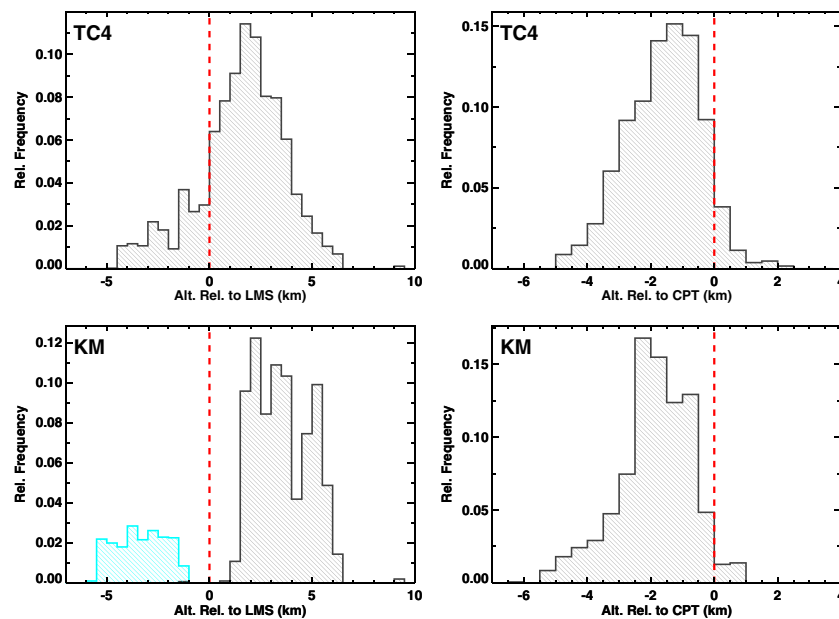


**Figure 9.** Distributions of transition layer air mass in relative altitude coordinates. Left column show the distribution of transition layer (purple/cyan in Figure 8) relative to the LMS. The right column show the transition layer relative to the CPT. The top row shows the result from the TC<sup>4</sup> data set. The bottom row shows result from the Kunming data set. The contribution to the transition layer from 7 August profile is shown in cyan.

distribution of transitional air mass in relative coordinates to the two critical levels, CPT and LMS, for both data sets. There are a number of ways to display these distributions. We have chosen to show the transition layer in the relative altitude space, i.e.,  $Z_r$  and

$$Z_r = Z - Z_{\text{CPT}} \quad \text{or} \quad Z_r = Z - Z_{\text{LMS}},$$

where  $Z$  is the geometric altitude of the measurements, and  $Z_{\text{CPT}}$  and  $Z_{\text{LMS}}$  are the altitudes of the colocated CPT and LMS, respectively. Note that  $Z_r$  is calculated individually for each profile, and it is a different function of  $Z$  for each profile.

A clear message of Figure 9 is that the tracer-based transition layer is consistent with the thermally defined TTL, i.e., the distribution of transitional air mass appear to be a compact layer in relative altitude coordinates, the layer is largely confined within the LMS and CPT. This is especially clear in the case of the TC<sup>4</sup> data where both the CPT and LMS mark the strongest discontinuity in the distribution. A subset of transition layer points appears below the LMS in both data sets and will be discussed in more detail later in this section. Using the full width at half maximum, the transition layer can be quantitatively described as approximately spanning ~4 km above the LMS and ~3 km below the CPT.

Results for the Kunming data set are similar to the TC<sup>4</sup> results, neglecting the subset contributed by the anomalous profile. The transition layer appears to be compact relative to both CPT and LMS, with a 3–4 km width. However, the transition layer appears to be approximately 1 km above the LMS and arguably 0.5 km below the CPT. This difference poses a question of how the thermodynamic structure and the convective outflow level differ between the ASM and the deep tropics.

The air mass associated with the anomalous profile (see cyan points in Figure 5) is identified by the cyan distribution in the bottom left panel of Figure 9. Note that this section of the distribution is entirely below the LMS. These air parcels are controlled by a different dynamical process, as revealed by the 200 hPa potential vorticity field (Figure 10) for 7 August 2009 (the day of sounding). A stratospheric filament, represented by the  $PV > 1$  potential vorticity unit (PVU) feature, is spinning off from a wave-breaking event over northeastern China. The sounding sampled an extremely dry middle to upper troposphere with enhanced ozone under the influence of this midlatitude intrusion. In this case, the upper tropospheric air masses depart from the background distribution due to mixing of upper tropospheric and midlatitude lower stratospheric air.

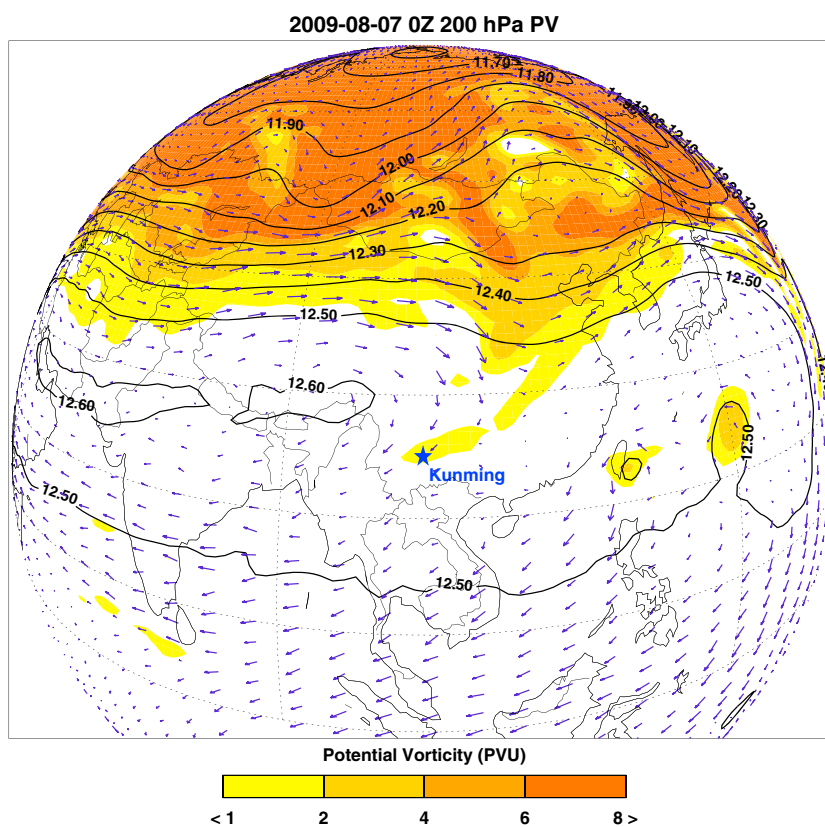


**Figure 10.** The 200 hPa PV field for August 7. A streamer of PV > 1 PVU over Kunming provides the dynamical background for the anomalous profile. Black contours represent the 200 hPa geopotential height (GPH, km) field, and wind vectors are shown in purple.

This air mass is below the local LMS, because the formation of this mixed stratosphere-troposphere air mass is driven by large-scale stratospheric dynamics rather than convection. This example also highlights the fact that the vertical profiles from the sounding data often reflect the influence of a 3-D flow. Therefore, tropical measurements can sometimes show the influence of the extratropics, which is especially true for the ASM region [Konopka *et al.*, 2010]. The process is also prevalent in the eastern Pacific during northern winter season [Vaugh and Polvani, 2000; Marcy *et al.*, 2007].

We also examined profiles that contributed to the distribution of transitional air below the LMS in TC<sup>4</sup> soundings. Although there were hints of similar influence, no clear evidence was found. The uncertainty of the LMS determination may be a factor, since the calculation of the LMS involves derivatives of fairly noisy data. Regardless of this uncertainty, we do not expect the CPT and LMS to be the “perfect” boundaries of air mass transition. The relative altitude distributions show that they capture the primary processes that control the air mass transition. There exist other processes, such as gravity waves and Rossby wave breaking in the quasi-isentropic directions, that may offset the thermal and tracer structures.

## 6. The Sensitivity of Results to the Choice of Tracer Cutoff Values

The use of tracer relationships is a well-developed method in stratospheric dynamics research. There is a long history of observations and a well-established theoretical framework [for review, see Plumb, 2007]. The application of the method in the UTLS, on the other hand, is largely empirical. The theoretical framework is lagging. A strong contrast between the stratospheric application and the UTLS work is that in the former relationships between the “long-lived” tracers are the main devices. In the latter, the chemical transition at the tropopause is best shown using a pair of stratospheric and tropospheric tracers, which can be of a range of lifetimes, from medium to short-lived, depending on the question under investigation. It is the sharp

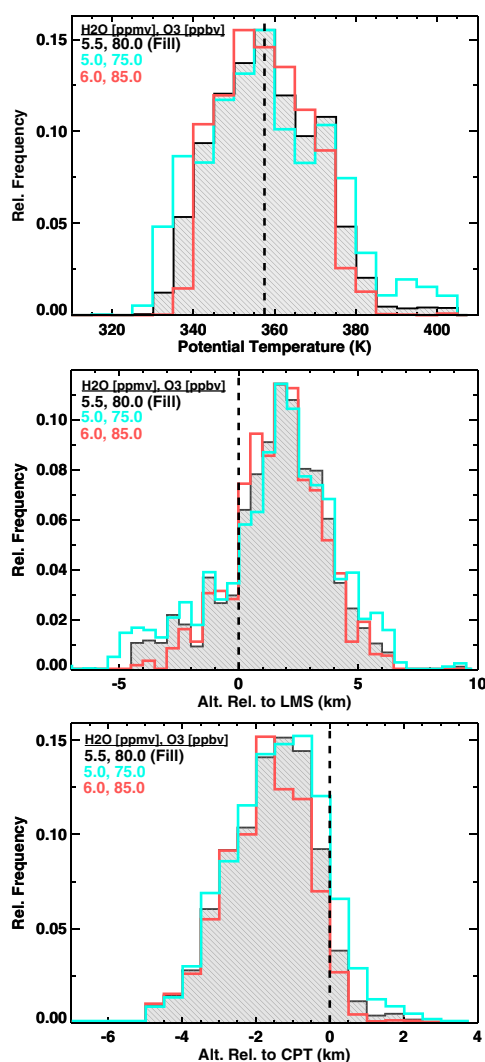


**Figure 11.** Sensitivity of transition layer determination to the tracer cutoff values. The analysis used the TC<sup>4</sup> data. The shaded distributions are the same as those shown in Figures 8 and 9. The red and cyan histograms show the distribution in potential temperature coordinates and the relative altitude to LMS and CPT, using a set of greater (red), and a set of lesser (cyan) background cutoff values, as specified by the color-coded legend.

lesser cutoff values produced a slightly wider distribution of the transition layer (by about 10 K), which does not change the conclusion that the transition layer lies between ~340 and 380 K. In the relative altitude space, neither of the cutoff values produces characteristic change. The transition layer remains very compact with respect to the two dynamical boundaries. The LMS and CPT still represent the lower and upper boundaries of the tracer-based transition layer. Although not shown, similar results are found for the Kunming data analyses.

## 7. Conclusions and Discussions

Tracer relationships have been effective diagnostic tools for identifying chemical transport and transport boundaries. In this work, we demonstrate the application of this method for characterizing a chemically “measurable” TTL and to examine whether the thermally and dynamically defined TTL boundaries mark the discontinuities of chemical composition. Our results show that the transition from troposphere to

change in the tracer’s source strength that largely determines the gradient of the tracer’s mixing ratio across the tropopause.

As an empirical method, the subjective choice of parameters, such as background cutoff values in the tracer space, based on trial and error is part of the analysis. Although the selection has a subjective component (inspection of the tropospheric ozone and the stratospheric water vapor distributions as discussed in section 4 for example), it should not be treated as arbitrary. A few conceptual considerations are discussed below.

When we initiate the background selection using the distribution of O<sub>3</sub>/H<sub>2</sub>O below/above the CPT, the statement has been made that we have chosen to examine the transition between the two layers (troposphere and stratosphere) that share the CPT as an imperfect boundary. The clear isolation of the two groups of air mass (as indicated by the near-Gaussian distribution) indicates that the boundary is physical and is able to maintain an air mass discontinuity. On the other hand, the lack of clear separation between the Gaussian and the tail in the distribution is a sign that the boundary is not robust and too diffusive (this is often the case in low-resolution large-scale models). For more discussions of how the tropopause definition should reflect the discontinuity in the air mass, see *Danielsen and Hipskind [1980]*.

Using the TC<sup>4</sup> data as an example, there is a clear separation between the Gaussian and the tail. However, the question of how sensitive results are to the choice of separation points remains. Figure 11 provides the results of sensitivity tests in which we compare the cutoff values used in the study (5.5 ppmv for H<sub>2</sub>O, 80 ppbv for O<sub>3</sub>) to a set of “greater” (6 ppmv, 85 ppbv) and a set of “lesser” (5 ppmv, 75 ppbv) cutoff values. As demonstrated in the figure, the distribution of transition layer air in the potential temperature space shows no characteristic change, i.e., the center and the width of the distribution are not changed, using the greater cutoff values. The

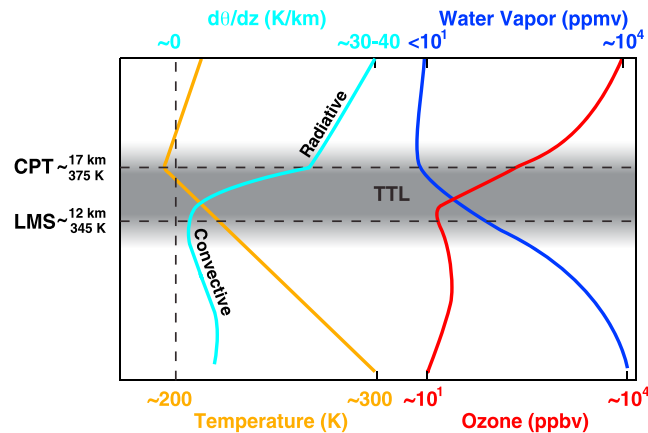


**Figure 12.** Schematic of TTL based on the thermal structure and chemical tracer relationships. The schematic highlights the change of  $O_3$  and  $H_2O$  at the two critical levels in the thermodynamic structure— $O_3$  begins to depart from its tropospheric background value at the LMS, and  $H_2O$  reaches its stratospheric background value near the CPT. The transitional air masses, as identified by the tracer-relationship, are well correlated with the LMS and the CPT.

stratosphere in the tropics can be clearly identified using the  $O_3$  and  $H_2O$  relationship. The results also show that the transition layer so identified is well correlated with the proposed TTL using the thermal definition [Gettelman and de F. Forster, 2002].

The main goal of this study, however, is not about providing another set of TTL boundary definition but to better understand the two existing conceptual models of TTL. The consistency between the tracer-identified transition layer and the thermal definition demonstrates that the transition from convectively dominated tropical upper troposphere to radiatively dominated tropical lower stratosphere is reflected in not only the temperature and static stability profiles but also the chemical composition

profiles. Figure 12 provides a schematic that highlights the key elements in this finding. These results furthermore suggest that the TTL so defined is a physically measurable layer and validate the controlling and maintenance mechanisms proposed by Thuburn and Craig [2002] in model studies.

This consistency of the chemical tracer-based transition layer with the thermal definition of the TTL does not invalidate the mass-flux definition of the TTL, which emphasizes the role of the TTL as a transport boundary. This exercise does, however, indirectly demonstrate the difficulty of connecting the mass-flux TTL with direct measurements, since the mass-flux TTL boundaries are not defined using local and instantaneous variables.

The results of this work also serve to connect the tropical transition layer (TTL) and the extratropical transition layer (ExTL). The combined analyses using tracer-tracer relationship and the dynamical boundaries have shown that in the extratropics, the thermal tropopause marks the center of the ExTL [Gettelman et al., 2011]. It is interesting to see that in the tropics, the similarly identified transition layer is associated with two dynamical boundaries: The CPT (a thermal definition of the tropical tropopause) marks its upper boundary and the LMS marks its lower boundary. This difference adds to the understanding that there are significant differences between the tropics and the extratropics in what processes control the transition from troposphere to stratosphere.

In this work, we used the  $O_3$ - $H_2O$  relationship because this tracer pair is available from balloon soundings that cover a sufficient vertical range of lower stratosphere, which is necessary for identifying background stratosphere in the tropics. It would also be beneficial to examine other tracer pairs, such as the  $O_3$ -CO relationship. Since  $H_2O$  has a significant sink in the tropopause region (dehydration), it would be interesting to see what new insight the  $O_3$ -CO pair may provide. Currently, high-resolution  $O_3$ -CO profile measurements in tropical UTLS are difficult to obtain. Future campaigns with new instrument technology and new platforms, including unmanned aerial vehicles, may make this analysis possible.

Using the Kunming measurements, we have shown that the transition layer in the ASM region shares similarities with that in the deep tropics, i.e., the tracer-identified transition layer in this region is also bounded by the CPT from above and the LMS from below. This result indicates that the UTLS chemical structure in the ASM region is tropical-like, as opposed to the extratropical UTLS structure where the transition layer (ExTL) is centered at the tropopause [Gettelman et al., 2011]. The transition layer over ASM is centered at a higher potential temperature. This higher level of ASM transition layer is consistent with previous analyses [Highwood and Hoskins, 1998; Dethof et al., 1999] that suggest the ASM as an alternative transport pathway for water vapor and tracers to enter tropical stratosphere. How this pathway competes

with the TTL is an area of active ongoing research [e.g., Randel et al., 2010; Ploeger et al., 2013]. Our result also indicates that the ASM transition layer, although qualitatively consistent with the TTL, may have different characteristics, i.e., is likely to have the influence of extratropical processes as shown in Figure 10. Due to the limitation of a small data set, we defer a more conclusive comparison to further analyses in future using more observations.

The two data sets used in this work serve to demonstrate the concept and test the method. In many respects, since the statistical base for this study is small, the results here are preliminary and prone to overinterpretation. It is desirable to expand this analysis to all available ozonesonde/CFH data sets. There are an increasing number of these data sets with planned future launches. Statistical behavior with a larger sample size is important for determining the TTL climatology. Characterization of the seasonal and longitudinal variability may also bring new insight into the controlling and maintenance mechanisms of the TTL.

## Appendix A: A List of Acronyms

TTL	tropical tropopause layer and tropical transition layer
LMS	level of minimum stability
CPT	cold point tropopause
LRT	lapse rate tropopause
STT	secondary tropical tropopause
UTLS	upper troposphere and lower stratosphere or upper tropospheric and lower stratospheric
ASM	Asian summer monsoon

## Acknowledgments

This work is supported by the National Science Foundation through its sponsorship to the National Center for Atmospheric Research. The SWOP campaign is supported by the National Basic Research Program of China (2010CB428602) and the National Natural Science Foundation of China (41175040). The authors thank Bill Randel, John Bergman, Cameron Homeyer, and three anonymous reviewers for helpful suggestions.

## References

- Atticks, M. G., and G. D. Robinson (1983), Some features of the tropical tropopause, *Q. J. R. Meteorol. Soc.*, **109**, 295–308.
- Bian, J., L. L. Pan, L. Paulik, H. Vömel, H. Chen, and D. Lu (2012), In situ water vapor and ozone measurements in Lhasa and Kunming during the Asian summer monsoon, *Geophys. Res. Lett.*, **39**, L19808, doi:10.1029/2012GL052996.
- Birner, T. (2006), Fine-scale structure of the extratropical tropopause region, *J. Geophys. Res.*, **111**, D04104, doi:10.1029/2005JD006301.
- Danielsen, E. F., and R. S. Hipskind (1980), Stratospheric-tropospheric exchange at polar latitudes in summer, *J. Geophys. Res.*, **85**(C1), 393–400, doi:10.1029/JC085iC01p00393.
- Dethof, A., A. O'Neill, J. M. Slingo, and H. Smith (1999), A mechanism for moistening the lower stratosphere involving the Asian summer monsoon, *Q. J. R. Meteorol. Soc.*, **125**, 1079–1106, doi:10.1002/qj.1999.49712555602.
- Fischer, H., F. G. Wienhold, P. Hoor, O. Bujok, C. Schiller, P. Siegmund, M. Ambaum, H. A. Scheeren, and J. Lelieveld (2000), Tracer correlations in the northern high latitude lowermost stratosphere: Influence of cross tropopause mass exchange, *Geophys. Res. Lett.*, **27**, 97–100.
- Folkens, I. (2002), Origin of lapse rate changes in the upper tropical troposphere, *J. Atmos. Sci.*, **59**, 992–1005.
- Folkens, I., M. Loewenstein, J. Podolske, S. Oltmans, and M. Proffitt (1999), A barrier to vertical mixing at 14 km in the Tropics: Evidence from ozonesondes and aircraft measurements, *J. Geophys. Res.*, **104**, 22,095–22,101.
- Folkens, I., C. Braun, A. M. Thompson, and J. White (2002), Tropical ozone as indicator of deep convection, *J. Geophys. Res.*, **107**(D13), 4184, doi:10.1029/2001JD001178.
- Fu, Q., Y. X. Hu, and Q. Yang (2007), Identifying the top of the tropical tropopause layer from vertical mass flux analysis and CALIPSO lidar cloud observations, *Geophys. Res. Lett.*, **34**, L14813, doi:10.1029/2007GL030099.
- Fueglistaler, S., A. E. Dessler, T. J. Dunkerton, I. Folkens, Q. Fu, and P. W. Mote (2009), Tropical tropopause layer, *Rev. Geophys.*, **47**, RG1004, doi:10.1029/2008RG000267.
- Gottelman, A., and P. M. de F. Forster (2002), A climatology of the tropical tropopause layer, *J. Meteorol. Soc. Jpn.*, **80**, 911–942.
- Gottelman, A., P. Hoor, L. L. Pan, W. J. Randel, M. I. Hegglin, and T. Birner (2011), The extratropical upper troposphere and lower stratosphere, *Rev. Geophys.*, **49**, RG3003, doi:10.1029/2011RG000355.
- Grise, K. M., D. W. J. Thompson, and T. Birner (2010), A global survey of static stability in the stratosphere and upper troposphere, *J. Clim.*, **23**, 2275–2292.
- Haynes, P. H., and T. G. Shepherd (2001), Report on the SPARC Tropopause Workshop. SPARC Newsletter, No.17, pp. 3–10.
- Hegglin, M. I., C. D. Boone, G. L. Manney, and K. A. Walker (2009), A global view of the extratropical tropopause transition layer from Atmospheric Chemistry Experiment Fourier Transform Spectrometer O<sub>3</sub>, H<sub>2</sub>O, and CO, *J. Geophys. Res.*, **114**, D00B11, doi:10.1029/2008JD009984.
- Held, I. M. (1982), On the height of the tropopause and the static stability of the troposphere, *J. Atmos. Sci.*, **39**, 412–417.
- Highwood, E. J., and B. J. Hoskins (1998), The tropical tropopause, *Q. J. R. Meteorol. Soc.*, **124**, 1579–1604.
- Holton, J. R., and A. Gettelman (2001), Horizontal transport and the dehydration of the stratosphere, *Geophys. Res. Lett.*, **28**, 2799–2802.
- Hoor, P., H. Fischer, L. Lange, J. Lelieveld, and D. Brunner (2002), Seasonal variations of a mixing layer in the lowermost stratosphere as identified by the CO–O<sub>3</sub> correlation from in situ measurements, *J. Geophys. Res.*, **107**(D5), 4044, doi:10.1029/2000JD000289.
- Kley, D., P. J. Crutzen, H. G. J. Smit, H. Vömel, S. J. Oltmans, H. Grassl, and V. Ramanathan (1996), Observations of near-zero ozone concentrations over the convective Pacific: Effects on air chemistry, *Science*, **274**, 230–233, doi:10.1126/science.274.5285.230.
- Kley, D., H. G. J. Smit, S. Nawrath, Z. Luo, P. Nedelec, and R. H. Johnson (2007), Tropical Atlantic convection as revealed by ozone and relative humidity measurements, *J. Geophys. Res.*, **112**, D23109, doi:10.1029/2007JD008599.
- Komhyr, W. D. (1969), Electrochemical concentration cells for gas analysis, *Ann. Geophys.*, **25**, 203–210.

- Konopka, P., J.-U. Grooß, G. Günther, F. Ploeger, R. Pommrich, R. Müller, and N. Livesey (2010), Annual cycle of ozone at and above the tropical tropopause: Observations versus simulations with the Chemical Lagrangian Model of the Stratosphere (CLaMS), *Atmos. Chem. Phys.*, **10**, 121–132, doi:10.5194/acp-10-121-2010.
- Lawrence, M. G., and J. Lelieveld (2010), Atmospheric pollutant outflow from southern Asia: A review, *Atmos. Chem. Phys.*, **10**, 11,017–11,096, doi:10.5194/acp-10-11017-2010.
- Marcy, T. P., et al. (2007), Measurements of trace gases in the tropical tropopause layer, *Atmos. Environ.*, **41**, 7253–7261.
- Palmén, E., and C. W. Newton (1969), *Atmospheric Circulation Systems*, International Geophysics Series, vol. 13, pp. 603, Academic Press, New York.
- Pan, L. L., W. J. Randel, B. L. Gary, M. J. Mahoney, and E. J. Hints (2004), Definitions and sharpness of the extratropical tropopause: A trace gas perspective, *J. Geophys. Res.*, **109**, D23103, doi:10.1029/2004JD004982.
- Pan, L. L., et al. (2007a), Chemical behavior of the tropopause observed during the Stratosphere-Troposphere Analyses of Regional Transport experiment, *J. Geophys. Res.*, **112**, D18110, doi:10.1029/2007JD008645.
- Pan, L. L., J. C. Wei, D. E. Kinnison, R. R. Garcia, D. J. Wuebbles, and G. P. Brasseur (2007b), A set of diagnostics for evaluating chemistry-climate models in the extratropical tropopause region, *J. Geophys. Res.*, **112**, D09316, doi:10.1029/2006JD007792.
- Paulik, L. C., and T. Birner (2012), Quantifying the deep convective temperature signal within the tropical tropopause layer (TTL), *Atmos. Chem. Phys.*, **12**, 12,183–12,195, doi:10.5194/acp-12-12183-2012.
- Pfister, L., H. B. Selkirk, D. O. Starr, K. Rosenlof, and P. A. Newman (2010), A meteorological overview of the TC4 mission, *J. Geophys. Res.*, **115**, D00J12, doi:10.1029/2009JD013316.
- Ploeger, F., G. Günther, P. Konopka, S. Fueglistaler, R. Müller, C. Hoppe, A. Kunz, R. Spang, J.-U. Grooß, and M. Riese (2013), Horizontal water vapor transport in the lower stratosphere from subtropics to high latitudes during boreal summer, *J. Geophys. Res. Atmos.*, **118**, 8111–8127, doi:10.1002/jgrd.50636.
- Plumb, R. A. (2007), Tracer interrelationships in the stratosphere, *Rev. Geophys.*, **45**, RG4005, doi:10.1029/2005RG000179.
- Randel, W. J., M. Park, L. Emmons, D. Kinnison, P. Bernath, K. A. Walker, C. Boone, and H. Pumphrey (2010), Asian monsoon transport of pollution to the stratosphere, *Science*, **328**, 611–613, doi:10.1126/science.1182274.
- Seidel, D. J., and W. J. Randel (2007), Recent widening of the tropical belt: Evidence from tropopause observations, *J. Geophys. Res.*, **112**, D20113, doi:10.1029/2007JD008861.
- Selkirk, H. B., H. Vömel, J. M. Valverde Canossa, L. Pfister, J. A. Diaz, W. Fernández, J. Amador, W. Stolz, and G. S. Peng (2010), Detailed structure of the tropical upper troposphere and lower stratosphere as revealed by balloon sonde observations of water vapor, ozone, temperature, and winds during the NASA TCSP and TC4 campaigns, *J. Geophys. Res.*, **115**, D00J19, doi:10.1029/2009JD013209.
- Sherwood, S. C., and A. E. Dessler (2001), A model for transport across the tropical tropopause, *J. Atmos. Sci.*, **58**, 765–779.
- Smit, H. G. J., et al. (2007), Assessment of the performance of ECC-ozonesondes under quasi-flight conditions in the environmental simulation chamber: Insights from the Jülich Ozone Sonde Intercomparison Experiment (JOSIE), *J. Geophys. Res.*, **112**, D19306, doi:10.1029/2006JD007308.
- Takahashi, H., and Z. Luo (2012), Where is the level of neutral buoyancy for deep convection?, *Geophys. Res. Lett.*, **39**, L15809, doi:10.1029/2012GL052638.
- Thuburn, J., and G. C. Craig (2000), Stratospheric influence on tropopause height: The radiative constraint, *J. Atmos. Sci.*, **57**, 17–28.
- Thuburn, J., and G. C. Craig (2002), On the temperature structure of the tropical stratosphere, *J. Geophys. Res.*, **107**(D2), 4017, doi:10.1029/2001JD000448.
- Toon, B., et al. (2010), Planning and implementation of the Tropical Composition, Cloud, and Climate Coupling Experiment (TC<sup>4</sup>), *J. Geophys. Res.*, **115**, D00J04, doi:10.1029/2009JD013073.
- Vömel, H., D. E. David, and K. Smith (2007), Accuracy of tropospheric and stratospheric water vapor measurements by the cryogenic frost point hygrometer: Instrumental details and observations, *J. Geophys. Res.*, **112**, D08305, doi:10.1029/2006JD007224.
- Waugh, D. W., and L. M. Polvani (2000), Intrusions into the tropical upper troposphere, *Geophys. Res. Lett.*, **27**, 3857–3860.